The Role of Tunneling in the Spectra of H_5^+ and D_5^+ up to 7300 cm^{-1}

Mark A. Boyer,[†] David C. McDonald II,[‡] J. Philipp Wagner,[‡] Jason E. Colley,[‡]

Dylan S. Orr,[‡] Michael A. Duncan,[*,‡] and Anne B. McCoy [*,†]

[†]*Department of Chemistry, University of Washington, Seattle, WA 98195, USA*

[‡]*Department of Chemistry, University of Georgia, Athens, GA, 30602, USA*

E-mail: maduncan@uga.edu; abmccoy@uw.edu

Phone: 206-543-7464

Abstract

The spectra for H_5^+ and D_5^+ are extended to cover the region between 4830 and 7300 cm^{-1}. These spectra are obtained using mass-selected photodissociation spectroscopy. To understand the nature of the states that are accessed by the transitions in this and prior studies, we develop a four-dimensional model Hamiltonian. This Hamiltonian is expressed in terms of the two outer H_2 stretches, the displacement of the shared proton from the center-of-mass of these two H_2 groups, and the distance between the H_2 groups. This choice is motivated by the large oscillator strength associated with the shared proton stretch and the fact that the spectral regions that have been probed correspond to zero, one, and two quanta of excitation in the H_2 stretches. This model is analyzed using an adiabatic separation of the H_2 stretches from the other two vibrations and includes the non-adiabatic couplings between H_2 stretch states with the same number of quanta of excitation in the H_2 stretches. Based on the analysis of the energies and wave functions obtained from this model, we find that when there is one or more quanta of excitation in the H_2 stretches the states come in pairs that reflect tunneling doublets. The states accessed by the transitions in the spectrum with the largest intensity are assigned to the members of the doublets with requisite symmetry that are localized on the lowest-energy adiabat for a given level of H_2 excitation.

Introduction

The H_5^+ molecular ion has long been of theoretical and experimental interest. In 1960 Jones and Simpson used H_5^+ as a test system for developing a model to study the effect of delocalization on IR intensity.[1] Two years later, Dawson and Ticknee identified a mass spectrometric signature of this ion in a hydrogen discharge.[2] In this report, they noted that Schaeffer and Thompson had proposed the existence of $H_2 \cdot H_3^+$ in their consideration of H/D exchange between H_3^+ and D_2.[3] Structurally, H_5^+ can be thought of as either a strongly bound complex between H_2 and H_3^+, where the binding energy is roughly 2200 cm^{-1},[4] or as a proton bound complex between two H_2 molecules. Much of the more recent interest in H_5^+ hinges on its role in astronomy, both as a bound species and as an intermediate in the proton transfer following a $H_2 + H_3^+$ collision.

Direct observation of interstellar H_5^+ has yet to be reported. However, observation of H_3^+ was first reported by Oka[5] in 1996, indicating that $H_2 + H_3^+$ collisions must occur. Laboratory measurements of the infrared spectrum of H_5^+ between 3400 and 4000 cm^{-1} were first reported more than thirty years ago by Okumura, Yeh, and Lee.[6] Subsequently Bae[7] reported a spectrum between 6400 and 7900 cm^{-1}. More recently, one of our groups recorded the mid-IR spectrum of H_5^+ over a larger range of photon energies (from 2500 to 4500 cm^{-1}) as well as the spectrum of D_5^+ between 1500 and 3500 cm^{-1}.[4] In this study, two additional transitions were observed in the H_5^+ spectrum and three peaks were reported for D_5^+. All of these studies exploited the fact that the dissociation energies of H_5^+ and D_5^+ relative to the $H_2 + H_3^+$ and $D_2 + D_3^+$ products are roughly 2230 and 2400 cm^{-1}, respectively. This allowed them to obtain an action spectrum for the ion of interest by monitoring the growth of the H_3^+ or D_3^+ mass channel following the photon absorption of a single photon. In addition, Cheng *et al.* reported far-IR spectra of H_5^+ and D_5^+, which were obtained through an IR-MPD (multi-photon dissociation) experiment using the FELIX free electron laser.[8] This study extended the region of spectral coverage down to 200 cm^{-1} for H_5^+ and between 699 and 2000 cm^{-1} for D_5^+. The spectra obtained in these more recent studies were compared to calculated spectra

evaluated using a vibrational configuration interaction approach (VCI).

The history of the assignment of the observed transitions is similarly rich. Due to the lack of a heavy atom, H_5^+ has been termed 'astructural'.[9] While the minimum energy geometry can be described as a complex of H_3^+ with H_2, where the shared proton lies on the axis that connects the centers of mass of the two outer H_2 groups and with the two H_2 groups lying in perpendicular planes, the barrier for proton transfer is well-below the zero-point energy in the vibration that corresponds to the displacement of the shared proton between the outer H_2 units.[4,10] The barrier for the hindered rotation of the outer H_2 groups is also low, and the ground state wave function is also delocalized in this coordinate.[10,11]

The lack of a simple zero-order model for the vibrations in H_5^+ along with the absence of a heavy atom and large changes in the bond lengths and frequencies of the outer H_2 stretches with displacement of the shared proton[12] makes assignment of the spectrum sensitive to the model used in making these assignments. For example, Okumura *et al.* assigned their spectrum based on harmonic frequencies obtained from a normal mode analysis by Yamaguchi *et al.*, which was based on the minimum energy geometry of the cluster.[13,14] This led to a nominal assignment of the peaks at 3532 and 3910 cm^{-1} to the fundamentals in the out-of-phase and in-phase combination of the outer H_2 stretches. Subsequently, Bae used a similar model to assign the higher-energy peaks as transitions to states with two quanta of excitation in the outer H_2 stretches along with zero or one quantum of excitation in the shared proton stretch. They also identified a lower-energy peak at 4230 cm^{-1}, which was assigned as a transition to a combination band involving the first excited state in the outer H_2 stretches with one quantum of excitation in the shared proton stretch.

More recently, diffusion Monte Carlo (DMC) studies have identified the most probable structure of H_5^+ as the D_{2d} saddle point structure.[10,15] Using this structure as the reference, VCI calculations of the spectra have been performed, and the resulting calculated spectra agree well with the vibrational predissociation and IRMPD spectra obtained for transitions above and below the dissociation limit for the ion, respectively.[4,8] Calculated peaks at 3560,

3950, and 4268 cm^{-1}, which are close in energy and intensity to the peaks in the measured spectrum, have been assigned to the out-of-phase outer H_2 stretch with combination bands involving the shared-proton stretch and the in-phase outer H_2 stretch. Assignment of features below 3000 cm^{-1} in H_5^+ is more complicated due to the large couplings between the shared proton stretch, the breathing ($H_2 \cdot H_2$ stretch) vibration, and the other lower frequency vibrations. Based on a combination of fixed-node DMC studies and two-dimensional calculations that focused on the shared proton stretch and the breathing vibrations, a model has been developed that anticipates a series of peaks in H_5^+ spanning from ∼350-2000 cm^{-1} which are assigned to a progression in the shared-proton with odd numbers of quanta of excitation. The wave functions for these states extend into the H_2+H_3^+ product channel and the nodes in the wave functions lie perpendicular to the reaction coordinate.[16]

The results of two- and four-dimensional calculations using either an adiabatic separation of the shared proton modes[17,18] or MCTDH[19,20] have shown that the major features of the spectrum can be reproduced by a reduced dimensional model that does not include displacements of the shared proton off of the axis that connects the outer H_2 groups and the internal-rotation of the ion. A later nine-dimensional MCTDH calculation has been able to reproduce the spectrum up to ∼7500 cm^{-1}.[21] Based on this calculation, peaks at 3528, 3944, and 4248 cm^{-1} have been assigned to the out-of-phase outer H_2 stretch, an H_3^+ breathing mode, and a transition to a state with a single quantum of excitation in the shared proton stretch combined with the out-of-phase outer H_2 stretch. The peaks at 6823, 7304, 7681, and 7905 cm^{-1} have all been assigned as two quanta in the outer H_2 stretches combined with 0, 1, 2, and 3 quanta in the shared-proton stretches. While this assignment is generally consistent with earlier studies, it is surprising that some of the above assignments seem to reflect excitation to totally symmetric excited states. Finally, comparison of the results of the nine- and four-dimensional MCTDH calculations shows that the calculated spectra are in fairly good agreement despite a shift in the energies that reflects the missing vibrational degrees of freedom in the lower-dimensional calculation.

Assignment of a calculated spectrum is necessarily sensitive to the choice of coordinates, the size of the basis, and the quality of the potential energy surface that is used. Furthermore, full-dimensional approaches, while providing the ability to reproduce a spectrum with high fidelity can suffer from a corresponding difficulty in interpretation, as teasing apart the contributions of many motions can be a challenging process. In the present study, we develop a four-dimensional model that reproduces the main features in the reported spectra of H_5^+ and D_5^+. This model is based on the observation that the assignments described above focus on the outer H_2 stretches, the shared proton stretch, and the H_2 breathing vibration. Consequently, this model includes only these four vibrational motions. The wave functions and energies derived from this treatment are analyzed in terms of an adiabatic separation of the high-frequency H_2 stretches and the lower-frequency shared proton and H_2 breathing vibrations. Couplings are introduced between states with the same total amount of excitation in the outer H_2 stretches. The combination of the reduced dimensionality and the further adiabatic separation of the high and low-frequency vibrations simplifies the assignment of the calculated transitions.

Spectra based on this four-dimensional model are compared to the previously reported spectra, as well as to our newly-reported spectra between 4850 and 7300 cm^{-1} for both H_5^+ and D_5^+. Based on the analysis of the resulting calculations we suggest a revised description of the assignments of the peaks in the spectra of these ions in which the states that are accessed correspond to the symmetry allowed combination bands involving the lowest-energy state with the appropriate excitation in the outer H_2 stretch in combination with states with increasing excitation in the shared proton stretch.

Theory

Before considering the results of this model, we start by describing the model itself. H_5^+ has nine vibrational degrees of freedom. Two describe the outer H_2 bond lengths, two provide

the distances between the shared proton and the centers of mass of each of the two H_2 group, and two more are the angles between the vectors that describe the outer H_2 bonds and the vector that connects the centers of mass of the two H_2 groups. The remaining three coordinates include the torsion angle between the two outer H_2 groups and the two coordinates that describe displacements of the shared proton off of the axis that connects the centers of mass of the outer H_2 groups. In the model presented below, we focus on the coordinates that describe the outer H_2 stretches (r_1 and r_2), and the distances between the shared proton and the centers of mass of each of the outer H_2 groups (R_1 and R_2). This choice of coordinates is similar to that used in prior 4D MCTDH work by Valdes and Prosmiti[19,20] as well as adiabatic treatment by Sanz-Sanz *et al.*[17] The remaining coordinates are constrained to their values in the D_{2d} reference geometry. Specifically, the three angles are all constrained to 90° and the shared proton is constrained to lie on the axis that connects the centers of mass of the outer H_2 groups. The D_{2d} structure and the four coordinates that are used in this study are depicted in Figure 1. This structure corresponds to a low-energy transition state structure on the potential,[12] which, while not the lowest energy structure, is the most probable structure of the ion when zero-point energy is taken into account.[10,15] The choice to focus on these four coordinates is motivated by the fact that the displacement of the shared proton between the two outer H_2 groups carries most of the oscillator strength and that the spectral regions of interest correspond to transitions involving excitation of the outer H_2 stretching vibrations. This choice is further justified by considering that the five omitted coordinates have different symmetries than these nominally bright vibrations and carry significantly less oscillator strength. While transitions involving the other five vibrations will certainly contribute to the spectrum, the zero-order bright states are expected to correspond to transitions in the shared proton stretch that build off of states with two or fewer quanta of excitation in the outer H_2 stretching vibrations.

Hamiltonian

Based on the structure of H_5^+ shown in Figure 1, the reduced dimensional Hamiltonian is given by

$$H(R_1, R_2, r_1, r_2) = \frac{p_{R_1}^2}{2\mu_{R_1}} + \frac{p_{R_2}^2}{2\mu_{R_2}} + \frac{p_{r_1}^2}{2\mu_{r_1}} + \frac{p_{r_2}^2}{2\mu_{r_2}} - \frac{p_{R_1} p_{R_2}}{m_{\mathrm{H}^+}} + V(R_1, R_2, r_1, r_2) \tag{1}$$

where μ_{r_i} represents the reduced mass of one of the outer H_2 groups, $m_{\mathrm{H}}/2$, while μ_{R_i} provides the reduced mass of the shared proton, with mass m_{H^+} and one of the outer H_2 groups, which has a mass of $2m_{\mathrm{H}}$

$$\mu_{R_i} = \left(\frac{1}{m_{\mathrm{H}^+}} + \frac{1}{2m_{\mathrm{H}}} \right)^{-1} \tag{2}$$

Because we calculate the spectra for the four isotoplogues of H_5^+ in which the four atoms that make up the outer H_2 groups are all the same isotope of hydrogen, we differentiate the mass of the shared proton from that of the atoms in the outer H_2 groups by using m_{H^+} and m_{H}, respectively.

To simplify the Hamiltonian, rather than using R_1 and R_2 to describe the position of the central proton we use

$$\begin{aligned} a &= \frac{R_1 - R_2}{\sqrt{2}} \\ s &= \frac{R_1 + R_2}{\sqrt{2}} \end{aligned} \tag{3}$$

This coordinate choice removes the kinetic coupling term from the Hamiltonian in Eq. 1, leading to

$$H(a, s, r_1, r_2) = \frac{p_a^2}{2\mu_a} + \frac{p_s^2}{2\mu_s} + \frac{p_{r_1}^2}{2\mu_{r_1}} + \frac{p_{r_2}^2}{2\mu_{r_2}} + V(a, s, r_1, r_2) \tag{4}$$

where

$$\mu_a = \frac{4m_{\mathrm{H}}m_{\mathrm{H}}^+}{4m_{\mathrm{H}} + m_{\mathrm{H}}^+} \tag{5}$$

$$\mu_s = 2m_{\mathrm{H}} \tag{6}$$

The potential term, $V(a, s, r_1, r_2)$, is constructed as a spline interpolation over an evenly spaced grid of electronic energies that consists of 60 points in R_1 and R_2 and 15 points in r_1 and r_2 evaluated at the MP2/aug-cc-pVTZ level of theory using the Gaussian[22] electronic structure package. In these calculations, R_1 and R_2 range from 0.461 Å to 3.461 Å and r_1 and r_2 range from 0.256 Å to 1.256 Å. It is important to note that the use of the aug-cc-pVTZ basis is necessary for these calculations as the use of the smaller aug-cc-pVDZ basis gives qualitatively different spectra which do not agree with the measured spectra for this ion. This surprisingly large sensitivity of the calculated spectrum to the basis set used for the electronic structure calculations reflects the very flat potential along a. When the aug-cc-pVDZ basis is used, the equilibrium structure corresponds to the D_{2d} structure shown in Figure 1, with $s_e = 1.50$ Å, while with the larger basis, there is a small barrier (73 cm^{-1}) in the D_{2d} geometry, and $s_e = 1.54$ Å. When we take one-dimensional cuts through these potentials along a at the appropriate value of s_e with the outer H_2 bond lengths constrained to their values in the minimum energy geometry, we find that the calculated anharmonic frequencies of the shared proton stretch are roughly 40% larger when the aug-cc-pVDZ basis is used (1000 cm^{-1}) compared to when aug-cc-pVTZ is used (674 cm^{-1}). While such one-dimensional calculations are not expected to provide accurate frequencies for this ion, the sensitivity of this frequency to the basis set used for the calculation anticipates the sensitivity of the higher-dimensional calculations to this choice.

The large sensitivity of the shape of these potential cuts to the basis set raises the question of what would happen if a larger basis were used, and we repeated the analysis using an aug-cc-pVQZ basis. In this case the equilibrium value of s is still 1.54 Å, the barrier height is slightly higher, 90 cm^{-1} and the anharmonic frequency becomes 683 cm^{-1}. These values can also be compared to those reported by Xie *et al.* based on CCSD(T)/aug-cc-pVTZ calculations where the barrier height is 48.4 cm^{-1} and $s_e = 1.54$ Å.

Adiabatic Separation of the High and Low Frequency Vibrations

To facilitate the interpretation of the results of these calculations and to reduce the size of the basis sets required to express the Hamiltonian matrix, the calculations are performed by employing an adiabatic separation of the high-frequency H_2 stretches and the low-frequency displacement of the shared proton between the two H_2 groups. This type of vibrational adiabatic separation has been used to study a number of molecular systems, going back to the work of Johnson and Reinhardt in their study of water.[23] Such a treatment has been shown to be an effective approach to decouple high- and low-frequency vibrational motions. In the present study, the states are described in terms of two sets of quantum numbers. The first set of quantum numbers provides the excitation of the outer H_2 stretch, ν_{H_2}. Since the H_2 stretch excitation is divided between the two outer H_2 oscillators, for each value of ν_{H_2}, there are $\nu_{H_2} + 1$ adiabatic states. These are identified by the letters A, B and C. The associated wave functions are obtained by solving the two-dimensional Schrödinger equation

$$H^{H_2}(a,s) = \frac{p_{r_1}^2}{2\mu_{r_1}} + \frac{p_{r_2}^2}{2\mu_{r_2}} + V(r_1, r_2; a, s) \tag{7}$$

for the $v_{H_2}+1$ wave functions, $\Phi_{v_{H_2},\alpha}(r_1, r_2; a, s)$, and the corresponding energies, $\mathcal{E}_{\nu_{H_2},\alpha}(a,s)$, at each set of values of a and s. In this notation, α represents the specific adiabatic state (A, B, C). In the absence of couplings among the adiabatic states, the wave functions and energies would be obtained by solving the Schrödinger equation based on

$$H^{H^+}_{\nu_{H_2},\alpha} = \frac{p_a^2}{2\mu_a} + \frac{p_s^2}{2\mu_s} + \mathcal{E}_{\nu_{H_2},\alpha}(a,s) \tag{8}$$

This approximation reduces the four dimensional problem to a pair of coupled two dimensional problems. Conceptually, this is analogous to creating a set of effective potential energy surfaces that are functions of the coordinates of the shared proton, which are obtained by averaging the four-dimensional potential over the wave functions for the outer H_2 stretches.

While computationally attractive, this separation is only valid when the adiabatic potential energy surfaces remain separated by significantly more than the frequencies of the low-frequency vibrations. This requirement holds for states that have different values of ν_{H_2}, but it is not satisfied by adiabatic states with the same value of ν_{H_2}. Thus non-adiabatic corrections need to be introduced to allow for couplings between these states. These corrections account for the observation that in some geometries, the eigenstates of the Hamiltonian in Eq. 7 show a strong dependence on the given value of a and s. These changes in the H_2 wave functions can be viewed as coming in two types. In the first, the average H-H distance and the width of the wave function adjust as the system shifts from H_5^+ to a structure that more closely resembles $H_3^+ \cdot H_2$. While important, this term will couple states with the same as well as different value of ν_{H_2}. It is also small compared to the resultant change in the nature of the vibrational wave function coming from changes in a near $a = 0$.

At $a = 0$, the D_{2d} symmetry of the ion requires that the vibrationally excited states in the outer H_2 stretches reflect this symmetry. For example, for $\nu_{H_2} = 1$ these states would be the in- and out-of-phase combinations of the states with one quantum of vibrational excitation in one of the H_2 bonds. As the shared proton shifts toward one of the outer H_2 units, the structure of the ion is better described as a complex of H_3^+ and H_2. As the H_2 stretch frequency in H_3^+ is lower than that of H_2, the two outer H_2 oscillators are no longer equivalent, and so the H_2 wave functions more closely resemble local mode states (as opposed to normal mode ones). The lower energy state will have the H_2 stretch in H_3^+ excited, and in the higher energy state the H_2 is excited. In the discussion that follows, we will describe

an approach for accounting for this contribution to the non-adiabatic couplings.

Evaluation of the Adiabatic States

Since we are focusing our analysis on the non-adiabatic couplings between states with the same value of the ν_{H_2} quantum number, we start by re-expressing the wave function as

$$\left|\nu_{H_2}, \alpha; a, s\right\rangle = \sum_{j=0}^{\nu_{H_2}} c_j^{\alpha}(a, s) \left|j, \nu_{H_2} - j\right\rangle \tag{9}$$

where the $\left|j, \nu_{H_2} - j\right\rangle$ states used in the expansion are obtained by performing a vibrational self-consistent field (VSCF) calculation to obtain a set of separable wave functions based on the Hamiltonian in Eq. 7 at the chosen value of (a, s) (See Supporting Information for details). The corresponding expansion coefficients, $c_j^{\alpha}(a, s)$ are obtained by evaluating the overlap between these wave functions and the eigenfunctions of Eq. 7, $\Phi_{\nu_{H_2},\alpha}(r_1, r_2; a, s)$, at the same value of a and s and with the same value of ν_{H_2}. The coefficients are then scaled to ensure that the $\left|\nu_{H_2}, \alpha; a, s\right\rangle$ states are normalized. With the expressions for the wave functions for the adiabatic states provided by Eq. 9, the matrix elements of the coupled Hamiltonian matrix are

$$H^{\nu_{H_2}}_{\alpha,j,k;\alpha',j',k'} = \sum_l c_l^{\alpha}(a_j, s_k) c_l^{\alpha'}(a_{j'}, s_{k'}) \left\langle a_j, s_k|T|a_{j'}, s_{k'}\right\rangle + \mathcal{E}_{\nu_{H_2},\alpha}(a_j, s_k)\delta_{\alpha,\alpha'}\delta_{j,j'}\delta_{k,k'} \tag{10}$$

where the dependence on a and s is expressed in a discrete variable representation (DVR).[24] We can then find the wave functions and energies of this Hamiltonian, noting that the wave functions, $\Psi_{\nu_{H_2},n}(a, s)$, will have contributions from the $\nu_{H_2} + 1$ values of α, that is

$$\Psi_{\nu_{H_2},n}(a, s) = \sum_{\alpha} \chi_{\nu_{H_2},n,\alpha}(a, s) \tag{11}$$

Given that adiabatic potential energy surfaces are used to obtain the wave functions

and energies, a similar adiabatic procedure is also used to obtain the intensities. This is accomplished by evaluating the matrix elements of the dipole surface between the adiabatic states that represent the various levels of excitation of the outer H_2 stretches as a function of a and s. Care must be taken to ensure that the phases of these adiabatic wave functions are consistently defined. These transition moments are then used to evaluate the matrix elements of the dipole moment in the adiabatic representation.

Numerical Details

All wave functions and energies in this study were obtained using a DVR. The underlying basis for these calculations has been described by Colbert and Miller.[25] The energies for the adiabatic potential surfaces were evaluated using 60 points in r_1 and r_2 with both coordinates ranging from 0.5 Å to 2.0 Å. The VSCF wave functions were evaluated using the same grid to facilitate the evaluation of the $c_j^\alpha(a,s)$ coefficients in Eq. 9. The evaluation of the matrix elements in Eq. 10 was performed using a two-dimensional DVR with 100 points in both s and a. For these calculations, a ranged from -2.45 Å to 2.45 Å and s ranged from 0.6 Å to 3.6 Å. All calculations were performed in Mathematica.[26]

Experimental Methods

The H_5^+ and D_5^+ cations were produced in a pulsed discharge ion source using needle electrodes mounted in the throat of a pulsed supersonic expansion of pure hydrogen.[27] Efficient cooling is obtained by pulsing the discharge for 10 μsec at the temporal center of a 300 μsec gas pulse. The ions are analyzed and mass-selected in a specially designed reflectron time-of-flight mass spectrometer.[28] The density of these selected ions is far too low for absorption spectroscopy, and therefore we employ photodissociation measurements. To accomplish this, the ions are excited with the tunable output of an optical parametric oscillator/amplifier (OPO/OPA) laser system (Laser Vision) which tunes smoothly throughout the 2000 – 4500 cm^{-1} mid-IR

and 4850 – 7300 cm^{-1} near-IR regions. Upon resonant excitation, dissociation proceeds by the elimination of H_2 (D_2), and the spectra are recorded with a digital oscilloscope (LeCroy) in the resulting H_3^+ (D_3^+) fragment ion channels.

Results and Discussion

Spectrum of H_5^+

To start, we consider the spectra for H_5^+, shown in Figure 2. The previously reported spectrum below 2000 cm^{-1}, obtained in an IRMPD study of the ion,[8] is shown by the grey-shaded region in the top panel of this figure. In the middle panel, we show the spectrum in the region of the fundamental in the outer H_2. This spectrum was obtained by single photon dissociation of the ion to $H_3^+ + H_2$.[4] Finally, in the bottom panel, previously unreported spectra are shown. The transitions at 6684 and 7159 cm^{-1} along with two additional features at 7490 and 7770 cm^{-1} have previously been reported by Bae and assigned to vibrations involving two quanta of excitation in the outer H_2 stretches.[7] The features between 4500 cm^{-1} and 6000 cm^{-1} have not been previously reported.

Below 3000 cm^{-1}

As noted in the introduction, the series of roughly equally spaced peaks below 3000 cm^{-1}, which are labeled I_a through I_g, can be attributed to a series of transitions from the ground state to states that each have an odd number of quanta in the shared proton stretch.[4,8,16] The associated motion can be thought of as the vibration of a delocalized proton between the two outer H_2 groups. As a result, the wave functions that correspond to excitation of this vibration have amplitude near the minimum in the potential as well as along the wells that correspond to the dissociation channels that lead to the formation of $H_3^+ + H_2$. This can be seen in the plots of the wave functions that were evaluated using the lowest energy adiabatic potential for this ion, shown in Figure 3. Excitations to the states plotted correspond to

features in the spectrum that carry intensity larger than 1 km mol^{-1}.

The wave functions associated with the states that are accessed in the transitions labeled I_a to I_g in Figure 2 are plotted in Figure 3, while the 24 lowest-energy states ($E < 3200$ cm^{-1}) are shown in Figure S7. Closer examination of these wave functions shows that the ones that carry larger intensities are characterized as being antisymmetric along a, and have significant amplitude and relatively few nodes in the region where the ground state wave function has amplitude. It is this nearly constant amplitude and relatively few nodes in the excited state wave functions in the configurations where the ground state has amplitude that leads to the surprisingly long progression seen in the calculated spectrum plotted in top panel of Figure 2. This calculation is based on a model in which only excitation in the shared proton is expected to have intensity (s, being a totally symmetric vibration, is not IR active).

This assignment is further supported by a comparison of the scaled results of the four-dimensional calculations, which are shown with red sticks in the top panel of Figure 2 and reported in Table 1 (information for the 24 lowest energy states provided in Table S2), with the recorded spectrum shaded in grey in the top panel of Figure 2. In this Table, the assignment of the number of quanta in the shared proton vibration is determined by the number of nodes in the calculated wave function that are perpendicular to the equipotential contours that extend into the product channel.

Displacements of the shared proton off of the axis that connects the centers of mass of the two outer H_2 groups and the rotation of the outer H_2 groups will lead to shifts in the frequency of the shared proton stretch. Therefore in Figure 2 the calculated transition frequencies have been scaled by 0.802. This scaling factor is the ratio of the calculated frequency of the fundamental in the shared proton stretch of 455 cm^{-1} and the value of 365 cm^{-1}, which is based on nine-dimensional multi-configurational time-dependent Hartree calculations.[19]

The need for this scaling factor can be seen by comparing the results of the current study

to the results of prior reduced dimensional (two- and four-dimensional) treatments and to those obtained by a full-dimensional treatment of the spectrum. For example, in Figure S5, we compare the present ones to those resulting from analysis of a two-dimensional potential surface, $V(a, s)$, which was obtained by minimizing the electronic energy with respect to the outer H_2 bond lengths.[16] While the relative intensities of the transitions are generally unaffected by the inclusion of the outer H_2 stretches in the calculation, the frequencies are notably lower when using the current four-dimensional approach. Similarly, Valdés and Prosmiti[19] compared the results of four- and nine-dimensional calculations over a comparable spectral range. They found that the fundamental in the shared proton stretch based on a similar four-dimensional calculation was at 505 cm^{-1} while a fully-coupled nine-dimensional calculation gave a value of 365 cm^{-1}.

Consistent with the experiment, the intensity of the transitions in this progression remains large until ∼2300 cm^{-1}, after which no additional transitions in this calculated progression carry significant intensity. Based on Figure 3, the excited state that corresponds to the I_g transition, which is the final state in this progression with significant intensity, has nine quanta of excitation in the shared proton vibration. An earlier study[8] identified this transition, which is observed at roughly 2600 cm^{-1}, as involving the second overtone in the shared proton stretch, which is consistent with the amplitude near the potential minimum showing three distinct nodes, and 68% of the amplitude being localized in this region of the potential.

Fundamental in the outer H_2 stretch

Next we consider transitions to states that involve one quantum of excitation in the outer H_2 stretches, shown with blue lines in the middle and lower panels of Figure 2 and identified as transitions II_a to II_h. The energies and wave functions for the states involved in these transitions are evaluated using the adiabatic potentials that correspond to the two states that have $\nu_{H_2} = 1$, and the calculations incorporate the non-adiabatic couplings between

these states as described above. To make comparisons to experiment, the position of the II_a peak is shifted to match the position of the feature near 3500 cm^{-1}, and the positions of the remaining peaks associated with transitions to states with $\nu_{H_2} = 1$ are scaled relative to peak II_a by the same 0.802 scaling factor used for the $\nu_{H_2} = 0$ peaks. Below 4500 cm^{-1} the agreement between the measured and calculated spectra is excellent. For the higher-energy features, the agreement is less satisfying, although there is clearly intensity in the calculated spectrum in the regions where there is intensity in the experiment. The missing features likely reflect excitation of degrees of freedom that are not included in the calculation, specifically the bends and internal rotation of the H_2 and H_3^+ subunits that make up the ion.

Given that we have obtained good agreement between the calculated and experimental spectra for peaks II_a to II_c, it is interesting to consider the assignments of the states involved in these transitions. By performing the calculations in an adiabatic representation, we are able to explore the contributions from the adiabatic states that involve the outer H_2 stretches when analyzing the nature of the states that contribute to the observed intensity above 3000 cm^{-1}. The wave functions that correspond to the blue peaks in Figure 2 that are labeled II_a to II_h are provided in Figure 4. The lower-energy adiabatic potential (State A) corresponds to the out-of-phase combination of the H_2 stretches when the shared proton is equidistant from the centers of mass of the two H_2 units. When the shared proton is displaced toward one of the outer H_2 units the lower energy state is the one for which the vibrationally excited H_2 molecule is closer to the shared proton and the H_2 molecule that is further from the shared proton is in its ground state. Overall, the wave function that is associated with the lower-energy adiabatic surface is antisymmetric with respect to exchange of the two outer H_2 units. The wave functions that are associated with the higher-energy adiabatic potential (State B) are symmetric with respect to this exchange, and when the shared proton is displaced toward one of the H_2 units the other H_2 is the one that is vibrationally excited. This behavior of the wave functions for the outer H_2 stretches can be seen in Figure 5.

The assignments for the labeled blue peaks in the spectrum are provided in Table 1. The

wave functions associated with these transitions are provided in Figure 4 (the wave functions for 24 lowest-energy states with $\nu_{H_2} = 1$ are plotted in Figure S7). As the calculation of the $\nu_{H_2} = 1$ wave functions considers two adiabatic surfaces these assignments include both a state label, expressed in terms of the number of nodes in the wave function along the shared proton stretch coordinate, and the fraction of the probability amplitude that is localized on each of the adiabatic potentials. As can be seen, the present assignment of the three peaks identified as II_a, II_b, and II_c departs from the assignments described above. In addition, the fact that we reproduce the spectrum without consideration of the bending vibrations makes the assignment of the II_c feature to an overtone in the bend unlikely. We find that the three peaks in the calculated spectrum are assigned to transitions to states that have most of their amplitude on the lower-energy adiabat (State A) with zero, two, and four quanta of shared proton excitation respectively. There is also a smaller but increasing contribution from the higher-energy adiabat (State B). The pattern continues for the transitions to higher energy states with one quantum of excitation in the outer H_2 stretches.

First Overtone in the outer H_2 stretch

A similar picture emerges for the transitions to states with two quanta of excitation in the outer H_2 stretches. The results of our analysis of the wave functions for these transitions are provided in Figure 6 and Table 1 (the wave functions associated with the 24 lowest-energy states with $\nu_{H_2} = 2$ are plotted in Figure S8). For these states, we have shifted the energies of the calculated transitions so that the peak identified as III_a is at the same frequency as the feature in the spectrum at 6684 cm^{-1}, and the relative positions of the $\nu_{H_2} = 2$ features are scaled using the same 0.802 scaling factor used for the peaks with $\nu_{H_2} = 0$.

In this case, the lowest-energy adiabatic surface (State A) corresponds to two quanta of excitation in the antisymmetric outer H_2 stretch. The second adiabat (State B) corresponds to a single quantum of excitation in each of the H_2 molecules. The third and highest-energy adiabat (State C) corresponds to two quanta of excitation in the symmetric outer H_2

stretch. It is notable that for these adiabats, States A and C are symmetric with respect to the exchange of the outer H_2 units while State B is antisymmetric with respect to this exchange. In this case, most of the amplitude remains on the lowest-energy adiabat, and the two observed transitions labeled III_a and III_b correspond to one and three quanta of excitation in the shared proton stretch, respectively.

As noted above, Bae[7] identified two additional features in the spectrum above 7300 cm^{-1} at 7490 and 7770 cm^{-1}, and the feature at 7490 cm^{-1} had larger intensity than the one at 7130 cm^{-1}. Based on the results provided in Figure 6 and Table 1, we find that the next two transitions involving states with two quanta in the outer H_2 stretches that carry intensity greater than 0.5 km mol^{-1} occur at 7341 and 7769 cm^{-1} and are less than half as intense as the ones labeled III_a and III_b. A comparison between that spectrum and our calculated spectrum over the same frequency range is provided in Figure S9. The agreement is generally good for the two lower-energy features, but the calculation fails to capture the intensity of the peak at 7490 cm^{-1}. The fact that intensity is observed in this region is not entirely surprising, although the peaks are larger than is anticipated by these calculations as well as the previously reported nine-dimensional MCTDH calculations.[21] The states that are accessed by calculated transitions in this spectral region are labeled III_c and III_d and follow the progression described above with five and seven quanta of excitation in the shared proton stretch.

Tunneling and the Assignment of Combination Bands

An interesting feature of the spectra with zero to two quanta of excitation in the outer H_2 stretches is the similarity between the energy spacings involving the first two peaks built off of the H_2 excitation with $\nu_{H_2} = 1, 2$ (384 cm^{-1},[4] and 475 cm^{-1}) and the fundamental frequency in the shared proton stretch[8] ($\sim$375 cm^{-1}). Based on this similarity in the spacings, it would be reasonable to conclude that the peaks labeled II_a and III_a involve transitions to excited states in the outer H_2 stretch, while II_b and III_b correspond to transitions to combination

bands with excitation in one of the outer H_2 molecules and one quantum of excitation in the shared proton stretch. Based on the analysis of the present calculations, this does not seem to be the case. This raises the question of how to reconcile the revised description of the assignments with the nearly constant spacing between these pairs of peaks.

If we perform the calculation of the spectrum based on our adiabatic potentials (without inclusion of the non-adiabatic coupling terms), the agreement between the experimental and calculated spectra deteriorates significantly (see Figure S12). To explore the role of non-adiabatic couplings, we focus on the one-dimensional minimum-energy path potentials (MEPs), shown in Figure 7, which are evaluated as functions of the displacement of the shared proton along the axis that connects the centers of mass of the two outer H_2 groups (a) by minimizing the energy as a function of the distance between the two outer H_2 groups (s) based on the two-dimensional adiabatic surfaces (see Figure S13). The reason for the large difference between the spectra obtained with and without consideration of the non-adiabatic couplings reflects the large change in the nature of $\Phi_{\nu_{H_2},\alpha}(r_1, r_2; a, s)$ near $a = 0$. In Figure 5 we plot these wave functions for all of the states used in this study when $a = 0.0$ and ± 0.495 Å with $s = 1.8$ Å. As is seen, even a small change in a shifts the wave functions from normal mode functions to nearly local mode functions with the vibrational excitation in only one of the outer H_2 units.

To better understand the effects of this coupling and to sort out the origin of the discrepancy in assignments, we develop a one-dimensional model that replicates the most important features of the four-dimensional system. To do this, we use the MEPs described above and shown in Figure 7 and then reintroduce the non-adiabatic couplings. From these cuts, we find that the barrier at $a = 0$ increases from approximately 50 cm^{-1} on the $\nu_{H_2} = 0$ surface to roughly 1000 cm^{-1} on the potential surface that corresponds to State A when $\nu_{H_2} = 2$. The increase in the barrier height with excitation of the outer H_2 stretches reflects the 805 cm^{-1} energy difference between the vibrational frequency of the two H_2 stretches when $a = \pm 0.495$ Å, reflecting the 1000 cm^{-1} frequency difference between the H_2 stretch frequency in an iso-

lated H_2 molecule and in H_3^+. When $a = 0$, the local H_2 frequencies are equal and the spacing between the two adiabatic surfaces is reduced to 112 cm^{-1}.

While the dependence of the energy difference between the two H_2 oscillator on the position of the shared proton is responsible for the barrier heights, the height of the tunneling barriers alone is not sufficient to yield the observed pattern in the energy levels. It is only when we introduce the non-adiabatic couplings that we obtain energy-level pattern that is consistent with high-barrier tunneling. Specifically, the energies of the six lowest-energy states with $\nu_{H_2} = 1$ come in pairs of closely spaced levels, and these pairs of levels are separated by larger energy gaps, as seen in Table S3. The spacing between the average energies of the states (0) and (1) and states (2) and (3) are calculated to be 372.5 and 377 cm^{-1} for the levels with $\nu_{H_2} = 1$ and 2. These values are both very close to the fundamental frequency of the shared proton stretch. A similar energy level pattern is obtained when we consider the energy levels obtained from the one-dimensional calculation based on the MEP potentials shown in Figure 7 in which the non-adiabatic couplings are considered. The origins of the large influence of the non-adiabatic terms in the Hamiltonian on the appearance of the tunneling doublets in the energy level pattern reflects the large change in the H_2 vibrational wave functions, shown in Figure 5, with small changes in a near $a = 0$. By analogy to electronic structure, this rapid change leads to large derivative coupling terms between the adibatic states near $a = 0$, or, if we had expressed the problem in a diabatic representation, weak couplings between the diabatic states that correspond to particular states associated with the outer H_2 stretches. As a result, although in the one-dimensional representation the two wells in the potentials shown in Figure 7 appear to be separated by modest barriers, the coupling between the wave functions localized in the two wells is weak due to the fact that the associated H_2 stretch wave functions associated with the adiabats when $\nu_{H_2} \neq 0$ at positive and negative values of a are orthogonal to each other (see Figure 5).

This tunneling behavior is further manifested in the projections of the vibrational wave functions onto a, shown in Figure S11, and in the wave functions obtained from the one-

dimensional model, which are shown in Figure 8. As can be seen in the plots in Figure 8 and Figure S11, the pairs of wave functions plotted in the same panel have the same width and can be considered as the in- and out-of-phase contributions of pairs of wave functions, one localized at positive values of a and one at negative values of a. This is exactly the behavior one would expect for tunneling doublets. Additionally, as the energy is increased the widths of both members of the pairs of wave functions increases, as expected for a progression in the excitation of a specific vibration.

Taken together, the revised assignment of the transitions observed in the region of the fundamental in the outer H_2 stretches corresponds to transitions to the symmetric member of tunneling doublets with increased numbers of quanta in the shared proton stretch, with the shared proton shifted toward the H_2 molecule that is vibrationally excited. Likewise, for the transitions to states with two quanta in the outer H_2 stretches, the ones that carry intensity correspond to transitions to the antisymmetric member of tunneling doublets with increasing numbers of quanta in the shared proton stretch, with the shared proton shifted toward the H_2 molecule that is vibrationally excited.

Role of Torsion

Before concluding our discussion of the spectrum of H_5^+, we need to consider the role of the torsional motion on the spectrum. In addition to the shared proton stretch, the torsion of the outer H_2 units reflects a large amplitude vibration in this ion. Earlier studies have demonstrated that the ground state wave function is fully delocalized in this coordinate.[10,11] On the other hand, the results that have been presented so far are based on a cut through the potential with the torsion coordinate constrained to 90°. To check if the above results are sensitive to the value of the torsion angle used in the evaluation of the potential surface, we repeat our calculation of the spectrum using a value of 0° for the torsion angle, which corresponds to the structure shown in Figure S1. Comparing the spectra obtained for these two structures, we find that they are almost identical, as is shown in Figure S3. The fact

that the spectrum does not change when the value of the torsion angle is shifted from 90° to 0° suggests that while the torsion is indeed large amplitude, its motion is nearly completely decoupled from the other vibrations considered in this study. This is consistent with the results of earlier work using DMC.[29]

Comparison with D_5^+

We have also evaluated the spectrum for D_5^+, and the comparison between the calculated and recorded spectra are provided in Figure 9. The associated wave functions and assignments can be found in Figures S16-S18 and Tables S11-S13. The calculated spectra in Figure Figure 9 have been shifted and scaled using a procedure that is analogous to that used to adjust the calculated spectrum for H_5^+, and the parameters can be found in Table S1. The agreement between the calculated and measured spectra is generally very good, especially when we consider that the transition near 2500 cm^{-1} is near the dissociation threshold for this ion. A similar difference between the calculated and measured intensity of this transition has been noted by Valdés and Prosmiti based on their nine-dimensional MCTDH calculation of the spectrum of the ion.[21] Since the ions are only detected when the vibrationally excited population dissociates into D_2 and D_3^+ fragments, the diminished intensity in the spectrum compared to calculation is consistent with this excited sate having an energy that is close to the dissociation energy of the ion.

In addition to the previously reported spectra, shown in the upper two panels of Figure 9, we also report the spectrum from 4830 - 7300 cm^{-1} in the bottom panel. This spectrum contains four peaks at 4860, 5220, 5495, and 5688 cm^{-1}. Our calculated spectrum agrees well with the experiment with respect to the positions of these peaks, but has some notable differences with respect to the intensities. The difference in intensity compared to the peak at 4860 cm^{-1} can be attributed to the laser power in the experiment in this region being diminished relative to the region above ∼5000 cm^{-1}. A more notable difference is the intensity of the peak around 5495 cm^{-1}. In both H_5^+[7] and D_5^+ this third peak has the largest

intensity of the four peaks in the spectral regions near the overtone in the outer H_2 or D_2 stretches. Comparing the H_5^+ and D_5^+ spectra, we find that they are very similar once the frequency scale for the D_5^+ spectrum are multiplied by roughly $\sqrt{2}$. It is notable, therefore, that for H_5^+ the nine-dimensional MCTDH calculations show the same difference in intensity for this third peak.[21] A possible explanation for this discrepancy between the calculated and measured intensities is that neither calculation fully accounts for the rotation of the H_3^+ fragment.

Given the otherwise good agreement of the frequencies it is interesting to analyze the wave functions that we have obtained for D_5^+. As we found for H_5^+, the states that are accessed by the transitions to states with $\nu_{D_2} = 2$ have most of their amplitude on State A with increasing quanta of excitation in the shared proton stretch. In the case of the lowest energy bright state the tunneling splitting between this level and the one with no quanta of excitation in the shared proton stretch is less than 1 cm^{-1}. This allows us to explore the relative sizes of the anharmonicity of the H_2 and D_2 stretches based on the frequencies of the lowest energy transition that carries in intensity, which corresponds to excitation of one or two quanta of excitation in the outer H_2 or D_2 stretch.

$H_2D^+H_2$ and $D_2H^+D_2$

Much of the spectroscopy of H_5^+ can be interpreted in terms of the motions of an excess proton that is trapped between two H_2 molecules. While such a bonding structure is not uncommon, and protonated dimers of water,[30] CO_2,[31] and N_2,[32] for example, have displayed similar structures, H_5^+ is unusual in that deuteration not only has a large impact on the amplitude of the shared H^+ or D^+ motion, it also doubles the mass of the molecular cage that traps the excess proton. This in turn has a significant effect on the amplitude of the breathing motion of the outer H_2 or D_2 molecules, which can be seen to be strongly coupled to the shared proton stretch, given the curvature of the ground state wave function shown in the upper left panel of Figure 3. As a result, full deuteration of the ion not only affects

the amplitude of the shared proton stretch motion, it also limits the extent to which the wave functions extend into the $H_3^+ + H_2$ product channel. Both of these factors lead to the observed shorter progression in the shared proton stretch in D_5^+ compared to H_5^+.

To sort out the contributions to the spectrum from deuterating the central proton as opposed to deuteration of the outer H_2 groups, we also calculate the spectra for $H_2D^+H_2$ and $D_2H^+D_2$, where the isotopically unique atom is the central proton. The resulting spectra are provided in Figures S22 and S28 while the corresponding energies and wave functions are reported in Tables S14-S16 and Figures S23-S25 for $H_2D^+H_2$ and Tables S17-S19 and Figures S29-S31 for $D_2H^+D_2$. Comparing the spectra shown in Figures 2 and 9 to those shown in Figures S22 and S28, we find that the range of the progression in the shared proton stretch is correlated to the masses of the outer H_2 units, while the frequency of this vibration reflects the deuteration of the central proton.

This trend can be understood in terms of the similarity between the ground state wave function, $\Psi_{0,0}(a,s)$, and the excited state wave functions, $\Psi_{\nu_{H_2}>0,n}(a,s)$. To quantify this, we consider the contour of $\chi^2_{0,0,A}(a,s)$, as defined in Eq. 11, that contains 99% of the probability amplitude. By evaluating the integrated area of each $\chi^2_{\nu_{H_2},n,\alpha}(a,s)$ over this region, $\xi_{\nu_{H_2},n,\alpha}$ (see Tables S3, S12, S15, and S18), and then evaluating

$$\Xi_{\nu_{H_2},n} = \sum_{\alpha} \xi_{\nu_{H_2},n,\alpha} \tag{12}$$

we are able to quantify the degree to which each state is localized near the minima in the potential. To explain the trend we evaluate $\Xi_{n,\nu_{H_2}}$ for the three states with $\nu_{H_2} = 1$ labeled II_a, II_b, and II_c in Figure 2 which correspond to the wave functions $\Psi_{1,0}(a,s)$, $\Psi_{1,2}(a,s)$, and $\Psi_{1,4}(a,s)$. For all four deuterated analogs of H_5^+ considered $\Xi_{1,0} \approx 0.92$. However, for H_5^+ and $H_2D^+H_2$ we find that $\Xi_{1,4} \approx 0.65$, while for D_5^+ and $D_2H^+D_2$ we find that $\Xi_{1,4} \approx 0.78$. This indicates that the wave functions for D_5^+ and $D_2H^+D_2$ remain significantly more localized near the minima in the potentials as the shared proton is excited. This reflects a difference

in the adiabatic potentials obtained when the outer units are H_2 as opposed to when they are D_2. The ability of the shared proton wave function to extend further away from the minima when H_2 is the outer unit supports a longer progression by reducing the orthogonality with the ground state wave function. It is worth keeping in mind that as $\Psi_{1,n}$ has contributions from $\chi_{1,n,\mathrm{A}}$ and $\chi_{1,n,\mathrm{B}}$, $\Xi_{1,n}$ will have contributions from $\xi_{1,n,\mathrm{A}}$ and $\xi_{1,n,\mathrm{B}}$.

Conclusions

In this study, spectra of H_5^+ and D_5^+ from 4830-7300 cm^{-1} have been reported. We have explored the nature of the states that are accessed in these and previously reported spectra using a four-dimensional model Hamiltonian. The calculations were performed by adiabatically separating the outer H_2 modes from the shared proton motions and then introducing non-adiabatic coupling for states with the same amount of outer H_2 excitation. We find that much of the observed intensity reflects the excitation of the shared proton stretch as the wave function extends in to the $H_3^+ + H_2$ dissociation channel with zero, one, and two quanta of outer H_2 excitation. This work demonstrates the effectiveness of a coupled four-dimensional adiabatic treatment to modeling the vibrational excited states of the highly-fluxional H_5^+ and D_5^+ molecular ions.

Acknowledgement

A.B.M acknowledges support from the National Science Foundation (CHE-1619660 and OAC-1663636). M.A.D acknowledges support from the Chemistry Division of the National Science Foundation (CHE-1764111). Parts of this work were performed using the Ilahie cluster, which was purchased using funds from a MRI grant from the National Science Foundation (CHE-1624430). This work was also facilitated through the use of advanced computational, storage, and networking infrastructure provided by the Hyak supercomputer system and funded by the STF at the University of Washington.

Supporting Information Available

Description of SCF procedure; scalings used; enlarged versions of Figures 2 and 9; plots of all wave functions for H_5^+, D_5^+, $H_2D^+H_2$, and $D_2H^+D_2$; complete tables, frequencies, and intensities for H_5^+, D_5^+, $H_2D^+H_2$, and $D_2H^+D_2$; spectra coming from the uncoupled calculation; tables of frequencies and intensities coming from uncoupled calculation; adiabatic potential and transition moment surfaces used; minimum-energy paths for D_5^+; plots of projections of the probability amplitude for H_5^+, D_5^+, $H_2D^+H_2$, and $D_2H^+D_2$; plots of wave functions from one-dimensional calculations for D_5^+, $H_2D^+H_2$, and $D_2H^+D_2$;

References

(1) Jones, W. D.; Simpson, W. T. Calculation of Delocalization Contribution to Infrared Intensity. *J. Chem. Phys.* **1960**, *32*, 1747–1756.

(2) Dawson, P. H.; Ticknee, A. W. Detection of H_5^+ in the Hydrogen Glow Discharge. *J. Chem. Phys.* **1962**, *37*, 672–673.

(3) Schaeffer, O. A.; Thompson, S. O. The Exchange of Hydrogen and Deuterium in the Presence of Electrons and Ultraviolet Radiation. *Radiat. Res.* **1959**, *10*, 671.

(4) Cheng, T. C.; Bandyopadhyay, B.; Wang, Y.; Carter, S.; Braams, B. J.; Bowman, J. M.; Duncan, M. A. Shared-Proton Mode Lights up the Infrared Spectrum of Fluxional Cations H_5^+ and D_5^+. *J. Phys. Chem. Lett* **2010**, *1*, 758–762.

(5) Geballe, T. R.; Oka, T. Detection of H_3^+ in Interstellar Space. *Nature* **1996**, *384*, 334.

(6) Okumura, M.; Yeh, L. I.; Lee, Y. T. Infrared Spectroscopy of the Cluster Ions $H_3^+ \cdot (H_2)_n$. *J. Chem. Phys.* **1988**, *88*, 79–91.

(7) Bae, Y. K. Observation of High-Lying Vibrational Predissociation States of H_5^+. *Chem. Phys. Lett.* **1991**, *180*, 179–181.

(8) Cheng, T. C.; Jiang, L.; Asmis, K. R.; Wang, Y.; Bowman, J. M.; Ricks, A. M.; Duncan, M. A. Mid- and Far-IR Spectra of H_5^+ and D_5^+ Compared to the Predictions of Anharmonic Theory. *J. Phys. Chem. Lett* **2012**, *3*, 24.

(9) Fábri, C.; Sarka, J.; Császár, A. G. Communication: Rigidity of the Molecular Ion H_5^+. *J. Chem. Phys.* **2014**, *140*, 051101.

(10) Lin, Z.; McCoy, A. B. Investigation of the Structure and Spectroscopy of H_5^+ Using Diffusion Monte Carlo. *J. Phys. Chem. A* **2013**, *117*, 11725–11736.

(11) Sarka, J.; Fabri, C.; Szidarovszky, T.; Csaszar, A. G.; Lin, Z.; McCoy, A. B. Modeling Rotations, Vibrations and Rotational Couplings in Astructural Molecules: A Case Study Based on the H_5^+ Molecular Ion. *Mol. Phys.* **2015**, *113*, 1873–1883.

(12) Xie, Z.; Braams, B. J.; Bowman, J. M. Ab-Initio Global Potential-Energy Surface for $H_5^+ \rightarrow H_3^+ + H_2$. *J. Chem. Phys.* **2005**, *122*, 8790.

(13) Yamaguchi, Y.; Gaw, J. F.; Schaefer, H. F. Molecular Clustering About a Positive ion. Structures, Energetics, and Vibrational Frequencies of the Protonated Hydrogen Clusters H_3^+, H_5^+, H_7^+, and H_9^+. *J. Chem. Phys.* **1983**, *78*, 4074–4085.

(14) Yamaguchi, Y.; Gaw, J. F.; Remington, R. B.; Schaefer, H. F., III The H_5^+ Potential Energy Hypersurface: Characterization of Ten Distinct Energetically Low-Lying Stationary Points. *J. Chem. Phys.* **1987**, *86*, 5072–5081.

(15) Acioli, P. H.; Xie, Z.; Braams, B. J.; Bowman, J. M. Vibrational Ground State Properties of H_5^+ and its Isotopomers from Diffusion Monte Carlo Calculations. *J. Chem. Phys.* **2008**, *128*, 104318.

(16) Lin, Z.; McCoy, A. B. Signatures of Large-Amplitude Vibrations in the Spectra of H_5^+ and D_5^+. *J. Phys. Chem. Lett.* **2012**, *3*, 3690–3696.

(17) Sanz-Sanz, C.; Roncero, O.; Valdés, A.; Prosmiti, R.; Delgado-Barrio, G.; Villarreal, P.; Barragán, P.; Aguado, A. Infrared spectrum of H_5^+ and D_5^+ : The simplest shared-proton model. *Phys. Rev. A - At. Mol. Opt. Phys.* **2011**, *84*.

(18) Valdés, A.; Barragán, P.; Sanz-Sanz, C.; Prosmiti, R.; Villarreal, P.; Delgado-Barrio, G. Theoretical simulations of the vibrational predissociation spectra of H_5^+ and D_5^+ clusters. *Theor. Chem. Acc.* **2012**, *131*, 1–7.

(19) Valdés, Á.; Prosmiti, R. Theoretical Investigation of the Infrared Spectra of the H_5^+ and D_5^+ Cations. *J. Phys. Chem. A* **2013**, *117*, 9518–9524.

(20) Valdés, Á.; Prosmiti, R. First-Principles Simulations of Vibrational States and Spectra for H_5^+ and D_5^+ Clusters Using Multiconfiguration Time-Dependent Hartree Approach. *Spectrochim. Acta - Part A Mol. Biomol. Spectrosc.* **2014**, *119*, 26–33.

(21) Valdés, Á.; Prosmiti, R. Theoretical Predictions on the Role of the Internal H_3^+ Rotation in the IR Spectra of the H_5^+ and D_5^+ Cations. *Phys. Chem. Chem. Phys.* **2014**, *16*, 6217–6224.

(22) Frisch, M. J.; Trucks, G. W.; Schlegel, H. B.; Scuseria, G. E.; Robb, M. A.; Cheeseman, J. R.; Scalmani, G.; Barone, V.; Mennucci, B.; Petersson, G. A. et al. Gaussian. 09 Revision D.0. Gaussian, Inc., Wallingford, CT 2009.

(23) Johnson, B. R.; Reinhardt, W. P. Adiabatic Separations of Stretching and Bending Vibrations: Application to H_2O. *J. Chem. Phys.* **1986**, *85*, 4538–4556.

(24) Light, J. C.; Carrington, T. *Adv. Chem. Phys.*; Wiley-Blackwell, 2007; Chapter 4, pp 263–310.

(25) Colbert, D. T.; Miller, W. H. A Novel Discrete Variable Representation for Quantum Mechanical Reactive Scattering via the S-matrix Kohn Method. *J. Chem. Phys.* **1992**, *96*, 1982–1991.

(26) Wolfram Research, Inc., Mathematica, Version 11.2. Champaign, IL, 2017.

(27) Duncan, M. A. Infrared Laser Spectroscopy of Mass-Selected Carbocations. *J. Phys. Chem. A* **2012**, *116*, 11477–11491.

(28) Cornett, D. S.; Peschke, M.; LaiHing, K.; Cheng, P. Y.; Willey, K. F.; Duncan, M. A. A Reflectron Time-of-Flight Mass Spectrometer for Laser Photodissociation. *Rev. Sci. Instrum.* **1992**, *63*, 2177–2186.

(29) Marlett, M. L.; Lin, Z.; McCoy, A. B. Rotation/Torsion Coupling in H_5^+, D_5^+, H_4D^+, and HD_4^+ Using Diffusion Monte Carlo. *J. Phys. Chem A* **2015**, *119*, 9405–9413.

(30) Diken, E. G.; Headrick, J. M.; Roscioli, J. R.; Bopp, J. C.; Johnson, M. A.; McCoy, A. B. Fundamental Excitations of the Shared Proton in the $H_3O_2^-$ and $H_5O_2^+$ Complexes. *J. Phys. Chem. A* **2005**, *109*, 1487–1490.

(31) Douberly, G. E.; Walters, R. S.; Cui, J.; Jordan, K. D.; Duncan, M. A. Infrared Spectroscopy of Small Protonated Water Clusters, $H^+(H_2O)_n$ ($n = 2 - 5$): Isomers, Argon Tagging, and Deuteration. *J. Phys. Chem. A* **2010**, *114*, 4570–4579.

(32) Bandyopadhyay, B.; Cheng, T. C.; Duncan, M. A. Proton Sharing in Hydronium-Nitrogen Clusters Probed with Infrared Spectroscopy. *Int. J. Mass Spectrom.* **2010**, *297*, 124–130.

Table 1: Frequencies (in cm^{-1}), Intensities (in km mol^{-1}), and Assignments of the Labeled Peaks in Figure 2.

Label[a]	Frequency	Intensity	State A[b]		State B[b]		State C[b]	
	cm^{-1}	(km/mol)	$n^c_{H^+}$	Percent[d]	$n^c_{H^+}$	Percent[d]	$n^c_{H^+}$	Percent[d]
I_a	365	2321.20	1	100.00	–	–	–	–
I_b	904	180.41	3	100.00	–	–	–	–
I_c	1340	54.70	5	100.00	–	–	–	–
I_d	1692	26.03	7	100.00	–	–	–	–
I_e	1968	18.00	9	100.00	–	–	–	–
I_f	2174	29.49	11	100.00	–	–	–	–
I_g	2267	64.54	9	100.00	–	–	–	–
I_h	2834	2.41	17	100.00	–	–	–	–
I_i	2963	2.67	17	100.00	–	–	–	–
II_a	3520	332.33	0	94.30	1	5.70	–	–
II_b	3889	72.18	2	79.30	1	20.70	–	–
II_c	4192	19.93	4	54.80	1	45.20	–	–
II_d	4391	1.42	4	67.20	3	32.80	–	–
II_e	4818	2.44	8	52.40	3	47.60	–	–
II_f	4935	2.86	8	85.50	5	14.50	–	–
II_g	5084	5.41	9	78.90	3	21.10	–	–
II_h	5151	1.43	10	63.60	5	36.40	–	–
III_a	6685	10.29	1	97.30	0	2.30	1	0.40
III_b	7040	4.46	3	91.60	0	6.00	1	2.40
III_c[e]	7341	0.69	5	82.30	0	10.30	1	7.40
III_d[e]	7769	1.99	7	70.90	0	4.50	1	24.50
III_e[e]	7923	1.54	9	80.90	1	3.70	1	15.40
III_f[e]	8305	3.52	9	70.50	1	7.70	1	21.90

[a] As identified in Figure 2.
[b] The adiabatic states with the same ν_{H_2} in increasing energy as described in Eq. 9.
[c] Number of nodes along the proton transfer coordinate.
[d] Percentage of the probability amplitude associated with the adiabatic state.
[e] Not shown in Figure 2.

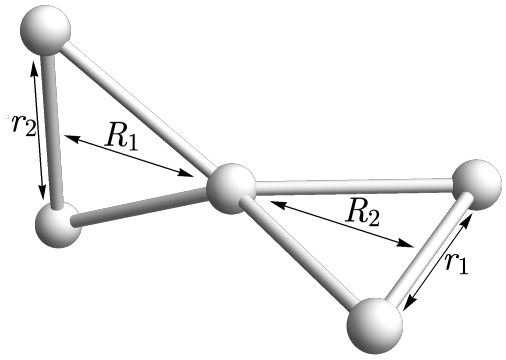

Figure 1: The D_{2d} structure of H_5^+ and the coordinates used for the calculations.

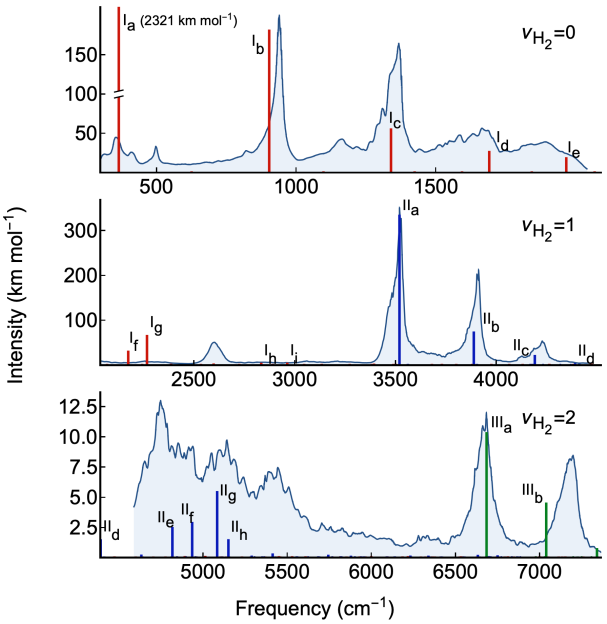

Figure 2: Experimental spectra (shaded grey) with calculated spectra (sticks) of H_5^+ overlain. The top panel compares the spectrum reported in Ref. 8 to the calculated transitions with $\nu_{H_2} = 0$ (red sticks). The middle panel compares the spectrum reported in Ref. 4 to the calculated transitions with $\nu_{H_2} = 0$ and $\nu_{H_2} = 1$ (red and blue sticks). The bottom panel compares our newly recorded spectrum reported to the calculated transitions with $\nu_{H_2} = 1$ and $\nu_{H_2} = 2$ (blue and green sticks). The positions of the transitions in the calculated spectrum have been shifted and scaled as described in the text and tabulated in Table S1. The intensity of I_a peak extends off the scale of the plot. A larger version of this figure can be found in Figure S2.

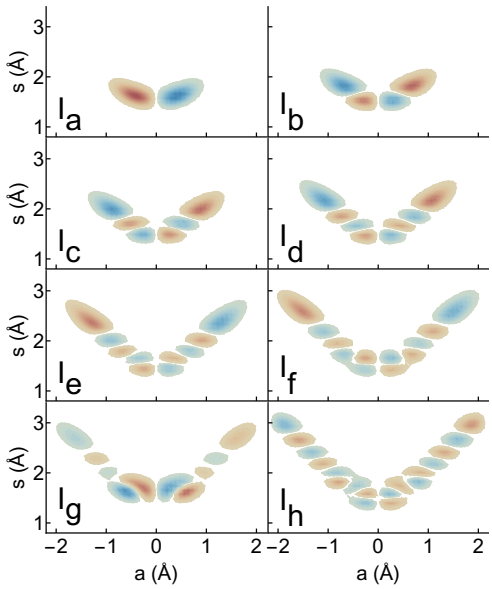

Figure 3: Wave functions for the states probed by transitions indicated by red sticks in Figure 2 labeled I_a to I_h. The energies, intensities and assignments of transitions to these states are provided in Table 1. As there is only one adibatic surface when $\nu_{H_2} = 1$, we only plot $\chi_{0,n,A}$ as defined in Equation 11.

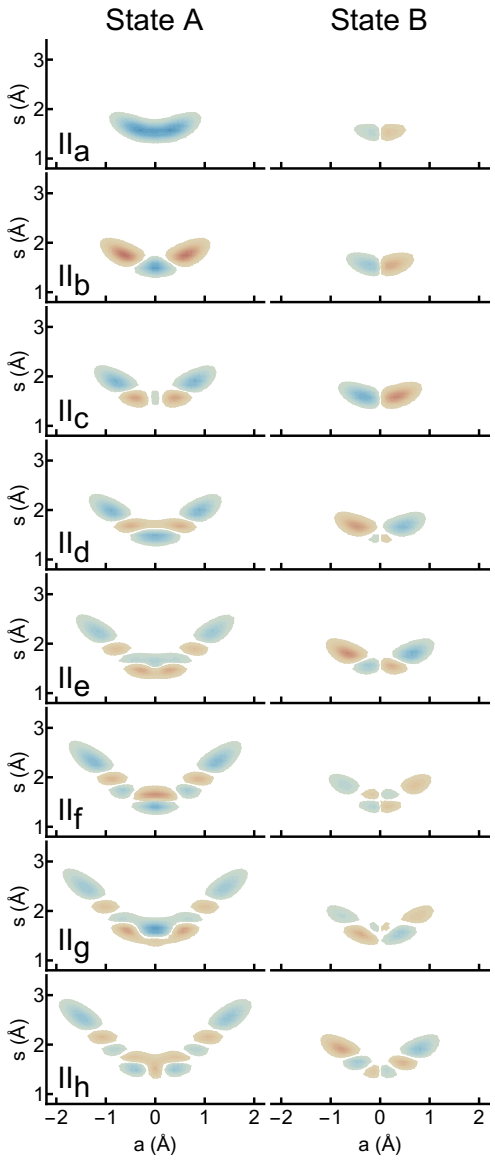

Figure 4: Wave functions for the states probed by transitions indicated by blue sticks in Figure 2 labeled II_a to II_h. The energies, intensities and assignments of transitions to these states are provided in Table 1. The wave functions are divided into the contributions from the two adiabatic states with one quantum in the H_2 stretch, $\chi_{1,n,A}$ and $\chi_{1,n,B}$ as defined in Equation 11, which are identified as State A and State B.

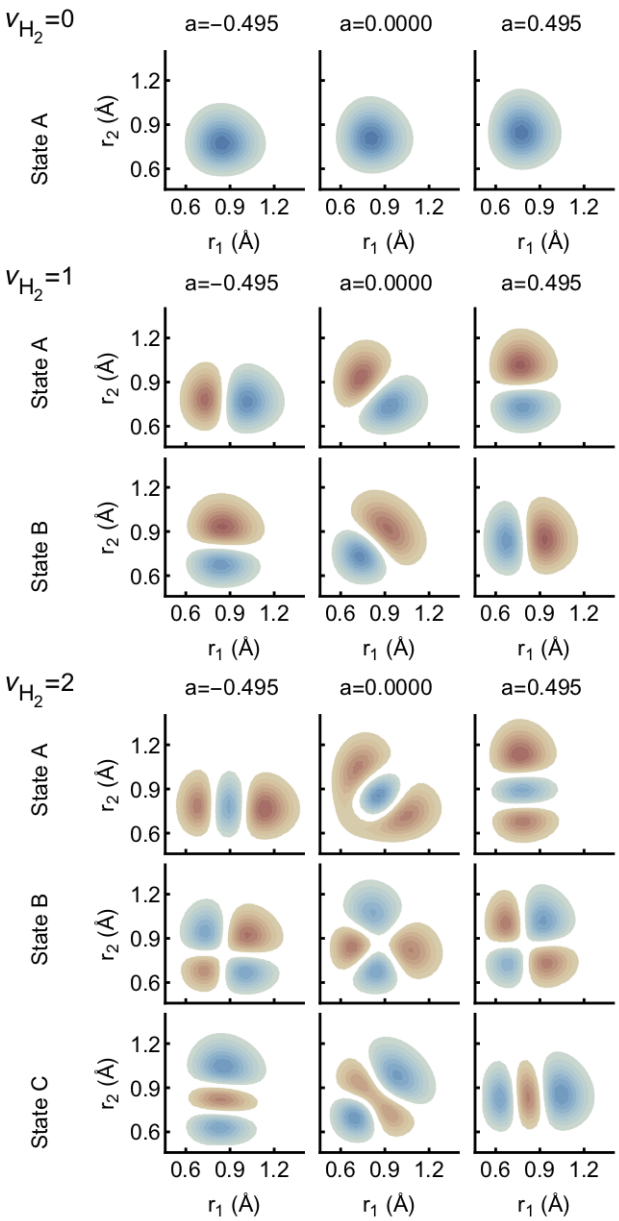

Figure 5: Plots of the H_2 wave functions for $a = 0$ and ± 0.495 Å at $s = 1.8$ Å for $\nu_{H_2} = 0, 1, 2$ for H_5^+. The wave functions when $a = \pm 0.071$ Å are provided in Figure S10.

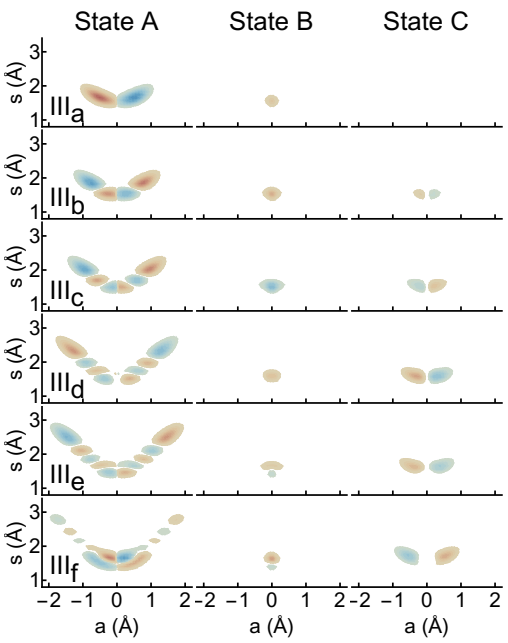

Figure 6: Wave functions for the states probed by transitions indicated by green sticks in Figure 2 labeled $\mathrm{III_a}$ and $\mathrm{III_b}$. The energies, intensities and assignments of transitions to these states are provided in Table 1. The wave functions are divided into the contributions from the three adiabatic states with two quanta in the H_2 stretch, $\chi_{2,n,\mathrm{A}}$, $\chi_{2,n,\mathrm{B}}$, and $\chi_{2,n,\mathrm{C}}$ as defined in Equation 11, which are identified as State A, State B, and State C.

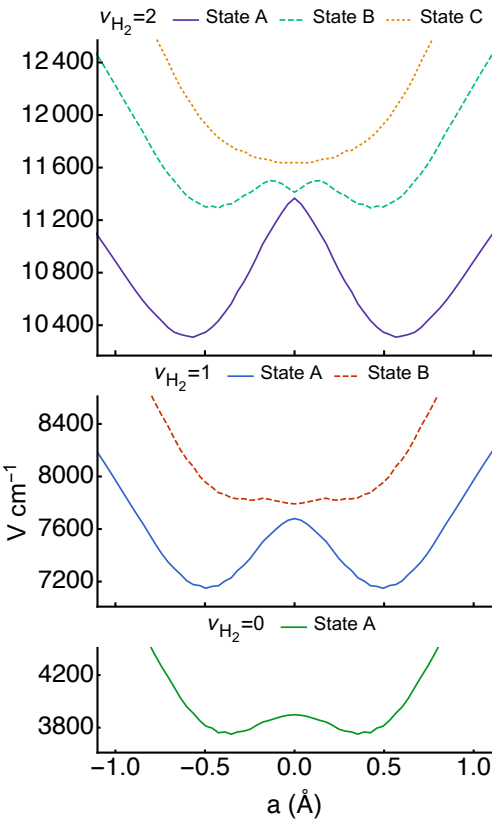

Figure 7: The minimum energy paths through the adiabats for $\nu_{H_2} = 0, 1, 2$. The curves are evaluated by finding the minimum in the potential with respect to s for each value of a.

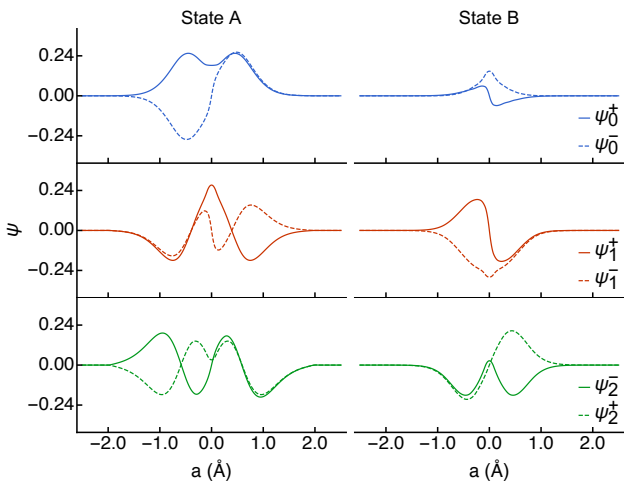

Figure 8: The one-dimensional wave functions associated with the six lowest-energy states evaluated using the $\nu_{H_2} = 1$ State A and State B minimum-energy curves shown in Figure 7 with non-adiabatic couplings introduced. The wave functions are divided into the contributions from the State A and State B adiabats. The wave functions for the two lowest-energy states are plotted in the top panel, those for the next two states are plotted in the middle panel, and the final two excited state plotted in the bottom panel.

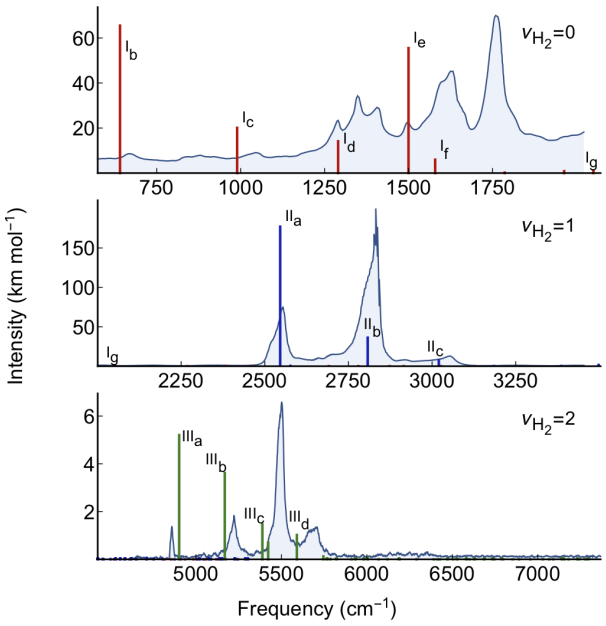

Figure 9: Experimental spectra (shaded grey) with calculated spectra (sticks) overlain for D_5^+. The top panel compares the spectrum reported in Ref. 8 to the calculated transitions with $\nu_{H_2} = 0$ (red sticks). The middle panel compares the spectrum reported in Ref. 4 to the calculated transitions with $\nu_{H_2} = 0$ and $\nu_{H_2} = 1$ (red and blue sticks). The bottom panel compares our newly recorded spectrum reported to the calculated transitions with $\nu_{H_2} = 1$ and $\nu_{H_2} = 2$ (blue and green sticks). The positions of the transitions in the calculated spectrum have been shifted and scaled as described in the text and tabulated in Table S1. A larger version of this figure can be found in Figure S15.

TOC Graphic

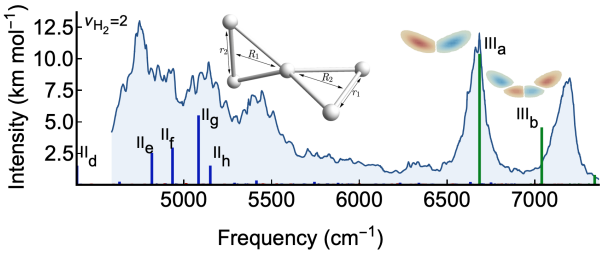
Intensity (km mol^{-1})
12.5
10.0
7.5
5.0
2.5
ν_{H_2}=2
II$_d$
II$_e$
II$_f$
II$_g$
II$_h$
III$_a$
III$_b$
5000
5500
6000
6500
7000
Frequency (cm^{-1})